TECHNICAL MEMORANDUM

168

Use of reduced Gaussian grids in spectral models

M. Hortal and A.J. Simmons

Research Department

June 1990

European Centre for Medium-Range Weather Forecasts
Europäisches Zentrum für mittelfristige Wettervorhersage
Centre européen pour les prévisions météorologiques à moyen

Abstract

Integrations of spectral models are presented in which the "Gaussian" grid of points at which the non-linear terms are evaluated is reduced as the poles are approached. A maximum saving in excess of one third in the number of points covering the globe is obtained by requiring that the grid length in the zonal direction does not exceed the grid length at the equator, and that the number of points around a latitude circle enables the use of a Fast Fourier Transform. Tests are reported for Eulerian and semi-Lagrangian barotropic models, mostly at T106 resolution, and a summary is given of experiments based on the T106 primitive-equation model used for operational forecasting at ECMWF. The results show that such a reduced grid can be used for short- and medium-range prediction (and presumably also for climate studies) with no significant loss of accuracy compared with use of a conventional grid which is uniform in longitude. The saving in computational time is between 20 and 25% for the T106 forecast model. There are also potential reductions in the memory requirement of the model and in the storage needed for the archiving of model results.

1. INTRODUCTION

Resolution is uniform over the sphere when triangular truncation is used for the global spectral representation of atmospheric variables, as is the case in the ECMWF spectral model, and in many other spectral models used routinely for weather prediction or climate studies. However, following the development of the transform method by Eliasen et al. (1970) and Orszag (1970), it is customary to integrate spectral models by carrying out much of the computation on a Gaussian grid which is regular in longitude, and almost regular in latitude, and which is thus far from uniform in its resolution over the sphere. For T106 resolution the longitudinal grid length is only 1841m at the Gaussian latitude closest to the pole, and for T213 the corresponding figure is 461m. Corresponding grid lengths close to the equator are about 125km and 63km respectively. A portion of the global grid for T106 resolution is shown in Fig. 1 in an azimuthal equal-area projection. The plotting fails to resolve individual grid-points as the pole is approached.

The possibility of integrating spectral models with fewer points around latitude circles away from the equator has been considered previously, but not pursued to the point of regular use. In particular, two studies were carried out at ECMWF. Machenhauer (1979) reported successful experiments with a 9-level spectral model. Later, Jarraud (personal communication) carried out a forecast in which the effect of using fewer points was simulated by setting to zero the values of associated Legendre functions when they fell below a certain threshold, this being based on the fact that in the Gaussian quadrature the contribution from polar latitudes to the tendencies of high-wavenumber spectral components can be smaller than machine accuracy. The results were sufficiently promising that some provision was made for using different numbers of points around different latitude circles in the coding of the operational ECMWF spectral model (Simmons and Jarraud, 1984). However, the work needed for operational implementation of the T63 spectral model in 1983 and T106 resolution in 1985 (Simmons et al., 1989) did not allow time for the use of a reduced number of points to be developed further.

It is timely now to reconsider this question, as model resolutions increase further, and polar points become even closer. In section 2 of this paper two alternative longitudinal distributions of points are introduced, and two choices of zonal truncation of input to or output from the Legendre transforms are discussed. Tests with the barotropic vorticity equation are described in section 3, where we investigate the performance of the reduced grids both for a conventional Eulerian integration scheme and for a semi-Lagrangian scheme. 10-day T106 forecasts using

the (Eulerian) operational ECMWF model are presented in section 4. Concluding discussion is given in section 5.

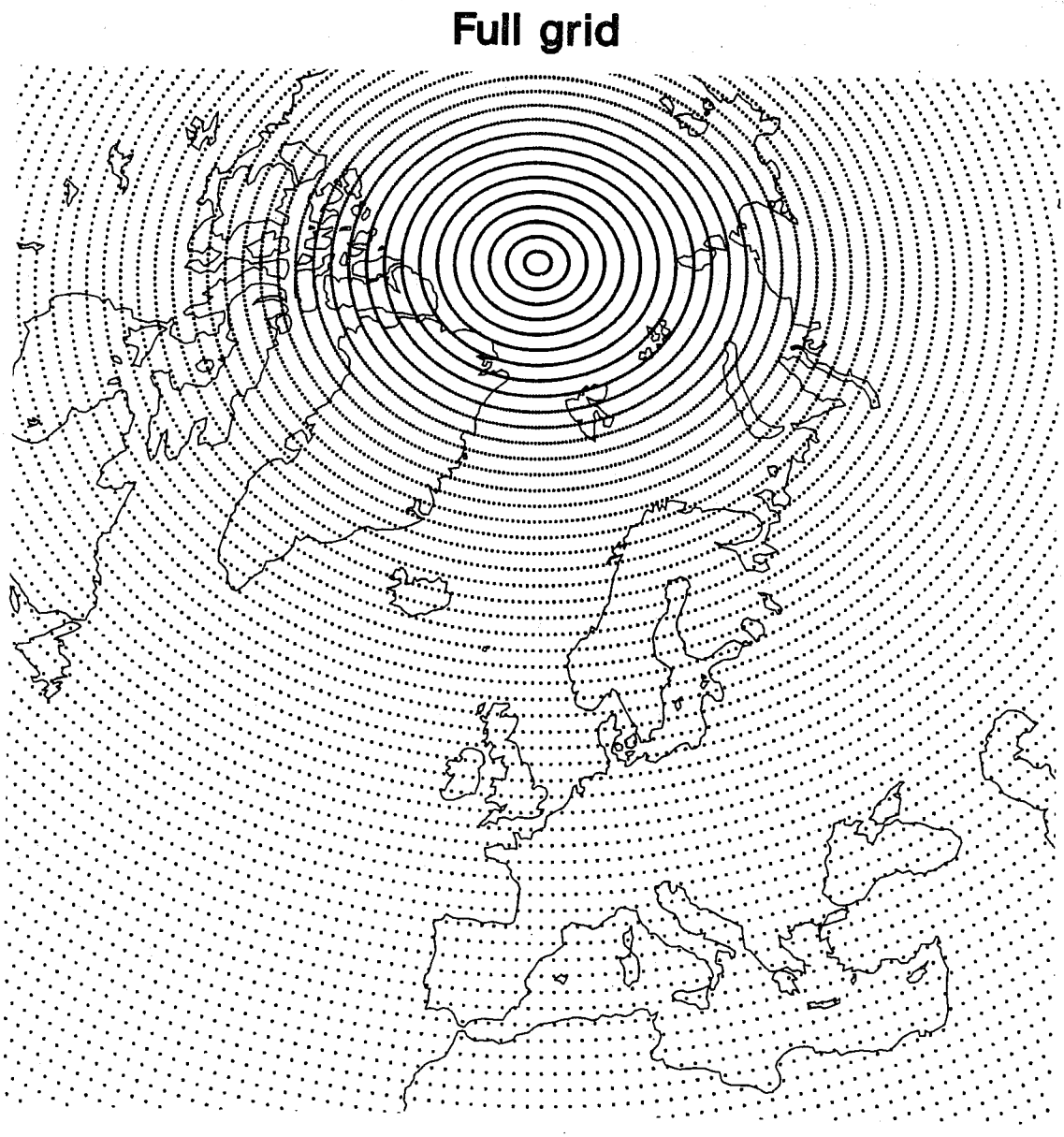

Fig. 1 The distribution of grid-points for the conventional T106 Gaussian grid.

2. THE REDUCED GRIDS AND LEGENDRE TRANSFORMS

The grids we study are based on the argument that if a certain grid-length is sufficient at the equator for use in the transform method with triangular truncation, then because of the isotropy of this truncation the same grid-length should in practice be sufficient everywhere, even if a precise alias-free calculation of quadratic terms is not achieved. The first grid to be considered, which we refer to as the "reduced grid", is chosen such that its points form a subset of the points of the standard Gaussian grid (the "full grid"). Grid-points are removed from latitude lines provided the resulting longitudinal grid-length does not exceed the grid-length at the Gaussian latitude nearest the equator (and provided there are sufficient points left for the Fast Fourier Transform (FFT) routine to work correctly). The reduction in points thus starts abruptly at the first line of latitude poleward of 60°. Fig. 2 illustrates the resulting distribution of points over middle and high latitudes for T106 resolution. For the globe as a whole, there are 21.5% fewer points in the reduced grid than in the full grid. The figure is 20.5% for T42 and 21.9% for T213. For T106, the grid length in the zonal direction varies between 125km and 60km.

The second grid, which is referred to as the "fully reduced grid", is defined as the minimal grid for which the longitudinal grid-length does not exceed the grid-length at the equatormost Gaussian latitude, and the number of points allows use of the FFT routine. This gives a much more uniform size for grid-boxes, but there can be a variable staggering of boxes from one latitude line to the next. These features can be clearly seen in the plot of T106 grid-points presented in Fig. 3. The calculation of points here assumes an FFT based on powers of 2, 3 and 5, which is the case for the ECMWF model. The zonal grid length varies between 125km and 114km, apart from the northernmost and southernmost rows, where the value is 100km. The number of points used for each latitude for the reduced and fully-reduced grids is set out in Table 1 for T106 resolution. There are 34.5% fewer points in the fully reduced grid than in the full grid in this case[1]. The corresponding figures are 33.8% for T42 and 34.9% for T213, and the figure for T106 increases only to 35% if factors of 7 are allowed in the FFT. The fully reduced grid is, incidentally, not very different from the grid proposed by Kurihara (1965) for finite-difference models, but does not exhibit the slight increase in grid-lengths as the pole is approached that occurs in the Kurihara grid.

---

[1] A limit on the saving in grid size is given by the factor:

$$\frac{\int_0^{\frac{\pi}{2}} (1 - \cos\theta) d\theta}{\int_0^{\frac{\pi}{2}} d\theta} = \frac{(\pi - 2)}{\pi} \approx 0.363$$

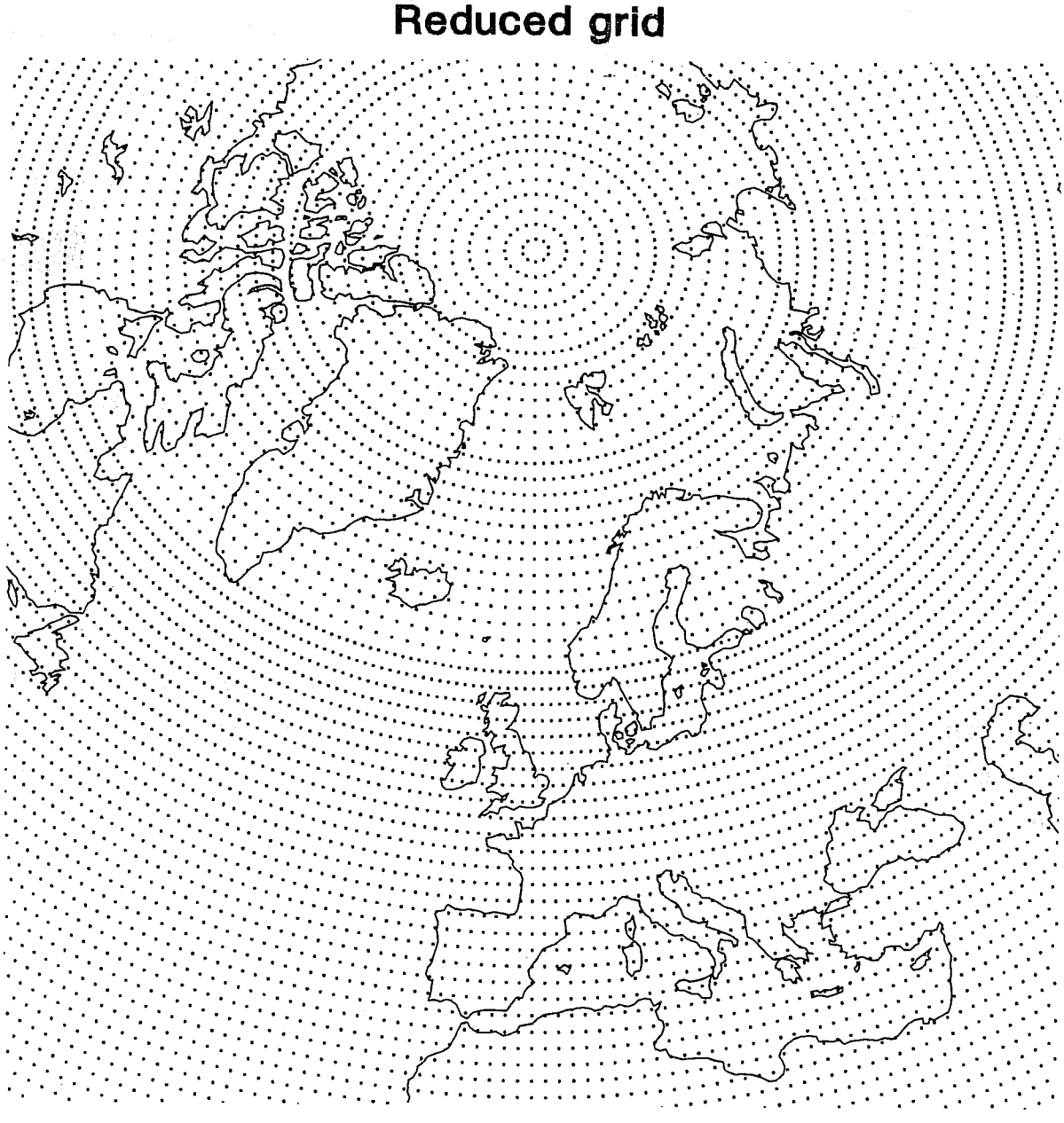

Fig. 2 The distribution of grid-points for the "reduced" T106 grid.

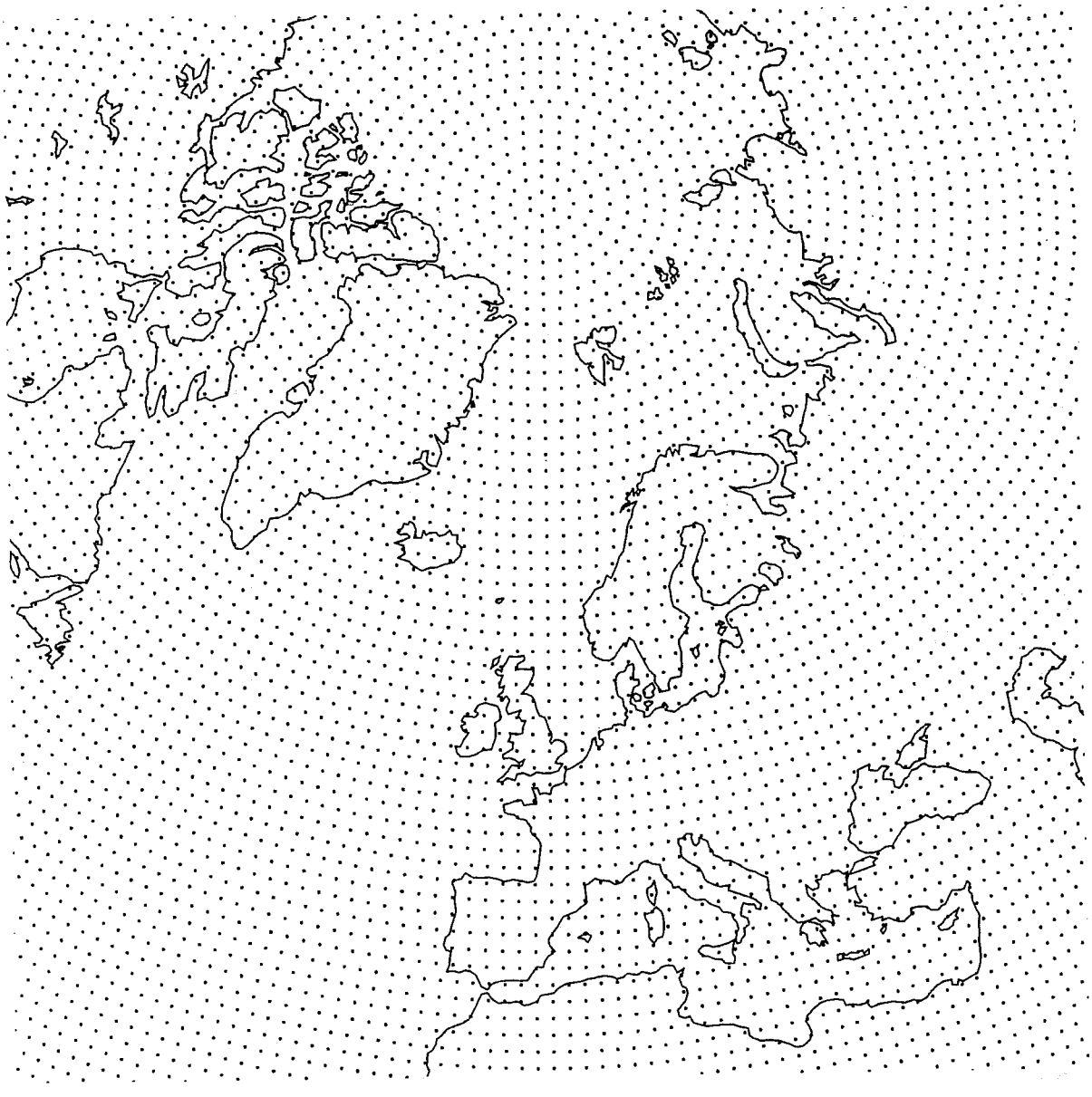

Fig. 3 The distribution of grid-points for the "fully reduced" T106 grid.

Lat	LONGITUDE POINTS Reduced	Fully reduced	Lat	LONGITUDE POINTS Reduced	Fully reduced
89.1	10	6	44.3	320	240
88.0	20	12	43.2	320	240
86.9	20	18	42.1	320	240
85.8	40	24	40.9	320	243 (256)
84.7	40	30	39.8	320	250 (256)
83.5	40	36	38.7	320	250 (256)
82.4	80	45	37.6	320	256
81.3	80	50	36.4	320	270 (288)
80.2	80	60	35.3	320	270 (288)
79.1	80	64	34.2	320	270 (288)
77.9	80	72	33.1	320	270 (288)
76.8	80	75	32.0	320	288
75.7	80	80	30.8	320	288
74.6	160	90	29.7	320	288
73.5	160	96	28.6	320	288
72.3	160	100	27.5	320	288
71.2	160	108	26.4	320	288
70.1	160	120	25.2	320	300
69.0	160	120	24.1	320	300
67.8	160	125 (128)	23.0	320	300
66.7	160	128	21.9	320	300
65.6	160	135	20.7	320	300
64.5	160	144	19.6	320	320
63.4	160	144	18.5	320	320
62.2	160	150	17.4	320	320
61.1	160	160	16.3	320	320
60.0	320	162	15.1	320	320
58.9	320	180	14.0	320	320
57.8	320	180	12.9	320	320
56.6	320	180	11.8	320	320
55.5	320	192	10.7	320	320
54.4	320	192	9.5	320	320
53.3	320	192	8.4	320	320
52.1	320	200	7.3	320	320
51.0	320	216	6.2	320	320
49.9	320	216	5.0	320	320
48.8	320	216	3.9	320	320
47.6	320	216	2.8	320	320
46.5	320	225	1.7	320	320
45.4	320	225	0.6	320	320

Table 1. The number of longitude points for each Gaussian latitude in the reduced and fully reduced grids for T106 resolution. For some latitudes a second set of figures is given in brackets for the fully reduced grid. These are the points used in the experiments with the full forecast model, where the choice of points for the full radiation calculation gave an extra constraint on the number of points that could be used.

For the fully reduced grid, there is a choice to be made in the range of zonal wavenumbers that are output from the inverse Legendre transforms and input to the direct Legendre transforms. Conventionally, if there are NLON longitude points for each latitude in the full grid, the Legendre transforms deal with zonal wavenumbers up to (NLON-1)/3 (42 for NLON=128, 106 for NLON=320, etc.). For the fully reduced grid, with NLN points at the latitude line under consideration, zonal wavenumbers up to (NLN/2-1) are produced by the FFT. We have considered the options either of truncating at wavenumber (NLN-1)/3, or of truncating at the minimum of (NLON-1)/3 and (NLN/2-1). Results from the former are referred to as from the "fully reduced model" and those from the latter are from the "fully reduced grid". The former option yields a bigger saving in the cost of the Legendre transforms[2] (about 22% as opposed to 14%) and in the requirement for work- and history-file storage. However, it gives rise to the greatest (albeit generally very small) differences from the conventional "full grid" approach in idealized calculations such as those presented in section 3.

As a preliminary indication of the error that can be introduced by the use of the reduced grids, these grids have been used in spectral/grid transforms of the T106 "envelope" orography used operationally at ECMWF (Jarraud et al., 1988), and of the corresponding T213 orography. The spectral forms of these orographies have been used to evaluate fields on the full Gaussian grid, the reduced grid and the fully reduced grid. Spectral fits of the fields defined on the reduced grids have been evaluated, and used to recompute orographies on the full grid. The maximum difference between the recomputed orographies on the full grid and the original orographies on this grid have been evaluated. For T106 these differences are only 0.1m for the reduced grid and 0.2m for the fully reduced grid. The difference rises to 6.8m when the more severe zonal truncation of the fully reduced model is used. For T213, the figure for the fully reduced grid is 0.1m, and that for the fully reduced model is 3.4m. These figures are quite negligible in comparison with the uncertainties which arise in the actual calculation of a model orography, as will be discussed further in connection with the T106 forecast experiments.

---

[2] An analytical expression for the saving in the Legendre trandforms with the fully reduced model is:

$$\frac{\int_0^{\frac{\pi}{2}} (1 - \cos\theta)^2 \, d\theta}{\int_0^{\frac{\pi}{2}} d\theta} = 1.5 - 4/\pi \approx 0.227$$

3. TESTS WITH THE BAROTROPIC VORTICITY EQUATION

A series of tests has been carried out using the barotropic vorticity equation. The integrations used either an Eulerian calculation of advection with a simple leapfrog time scheme or an interpolating semi-Lagrangian scheme based on the formulation and code of Ritchie (1988). It was straightforward to modify the latter for the irregular grids, since the cubic interpolation of fields to either a departure-point or the mid-point of a trajectory was achieved by carrying out four interpolations to the longitude of the point in question, one for each of the four nearest model latitude rows, followed by a single interpolation of the four resulting values in the latitudinal direction.

Both the Eulerian and semi-Lagrangian versions employed a weak time-filter (ν=0.02 in the nomenclature of Asselin, 1972) and some integrations also used a linear fourth-order horizontal diffusion with coefficient $10^{15}m^4s^{-1}$, the same value as used in the operational T106 forecast model. Most integrations were carried out to 10 days at T106 resolution with a timestep of 20 minutes for the Eulerian version and one hour for the semi-Lagrangian version. Some 50-day Eulerian integrations were performed using T42 resolution and a timestep of one hour. For parameter settings which gave stable integrations for the control model using the full Gaussian grid, no computational instability was found with either the reduced grid, the fully reduced grid or the fully reduced model. For plotting purposes, the spectral representation of fields was used to produce output on the full grid irrespective of the grid used for the dynamical calculations.

3.1 A Rossby-Haurwitz wave

The first test to be presented uses a Rossby-Haurwitz wave as initial conditions. The relative vorticity is defined by

$$\Omega\left(\frac{\sin\theta}{22} + 3(9/8)^4 \cos^8\theta' \sin\theta' \cos 8\lambda'\right)$$

where θ' and λ' are given by

$$\sin\theta' = \cos\theta \cos\lambda$$

and

$$\cos\lambda' = -\frac{\sin\theta}{\cos\theta'} \quad .$$

Ω is the planetary rotation rate, λ is longitude and θ is latitude. This corresponds to a conventional m=8, n=9 wave (m=zonal wavenumber, n=total wavenumber) with the pole rotated through 90°, plus a solid body rotation which is precisely such as to keep the wave pattern fixed in space. This is an exact, stationary solution of the non-linear barotropic vorticity equation, and any change in wave pattern during the course of an integration with the Eulerian version of the model must be due either to round-off errors in the computation, or due to the approximations introduced by using less than the full Gaussian grid. The particular initial conditions of an (8,9) wave with relatively large amplitude (maximum vorticity Ω) were chosen because the wave is known from the work of Hoskins (1973) to be unstable, which amplifies any effect of computational error.

A map showing the initial distribution of relative vorticity is shown upper left in Fig. 4, which also shows three distributions at day 10 using T106 resolution with no horizontal diffusion. These are for the full and fully reduced grids with the Eulerian version, and for the full grid with the semi-Lagrangian version. In each of the Eulerian cases shown (and in the corresponding cases of the reduced grid and the fully reduced model, not shown) differences between the 10-day forecast and the initial conditions are indiscernible. Quantitatively, the largest change in spectral coefficient between day 0 and day 10, normalized by the amplitude of the largest spectral coefficient, is found to be 0.39×10^{-9} when the full grid is used. The corresponding differences between the day-10 integration using the full grid and each of the other integrations are found to be 0.44×10^{-13} for the reduced grid, 0.23×10^{-12} for the fully reduced grid and 0.20×10^{-10} for the fully reduced model. For this special case a greater error is introduced by round-off errors than by any of the reductions in grid considered here. The same conclusion was found when the initial conditions were an (8,9) wave without the polar rotation. It should, however, be noted that the use of large-scale initial conditions facilitates the use of coarser grids. For example, in the case of the fully reduced grid the relevant zonal wavenumbers up to 9 will be treated exactly (apart from round-off errors) at all but the three rows nearest each pole (where there are 18 points or less per row).

In contrast, a distortion begins to be noticeable by day 10 in the semi-Lagrangian forecast shown in Fig. 4, and the wave pattern breaks down rapidly thereafter. At day 10, the corresponding semi-Lagrangian integration using the fully reduced grid (not shown) is very similar to the full-grid result presented in Fig. 4. The inability of the semi-Lagrangian version to maintain the structure of this particular wave-form much beyond day 10 is not viewed as an impediment to its use in practice, and indeed the maintenance of the steady solution for a week or more can

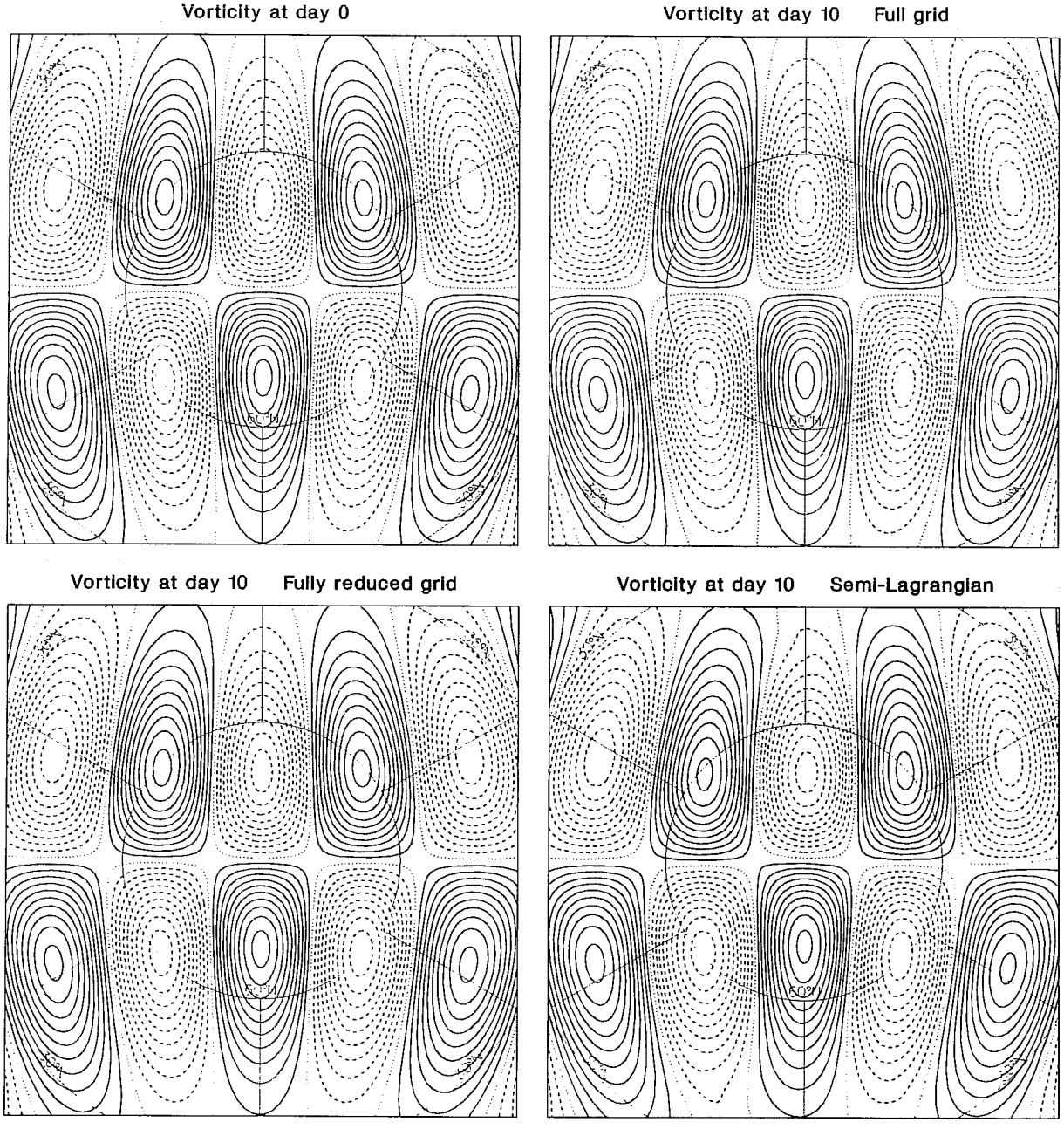

Fig. 4 The initial relative vorticity for a rotated (8,9) Rossby-Haurwitz wave, and fields at day 10 produced using the full and the fully reduced grid, for the Eulerian version of the model, and using the full grid for the semi-Lagrangian version. The resolution is T106. The contour interval here and in subsequent figures is one tenth the planetary rotation rate. The zero contour is dotted and negative contours are dashed.

perhaps be regarded as quite a success. The semi-Lagrangian results serve, however, to emphasize the insignificance of any change in structure brought about by the reductions in the grid.

The Eulerian integrations shown in Fig. 4, plus integrations using the reduced grid and the fully reduced model, have been carried out to 50 days for T42 resolution. Only beyond day 40 do distortions become apparent, and a quite comprehensive breakdown of the wave pattern occurs in all but one case by day 48, for which results are shown in Fig. 5. By this time the expected Rossby-wave instability has occurred in all but the case of the fully reduced model, for which breakdown is delayed. Some very small differences can be seen between the full-grid field and the fields from the reduced grid and (more particularly) the fully reduced grid, but it is clear that for these two model versions the impact of the grid reduction is still very much less than the large change from the initial state that has been brought about by round-off error. This is not the case when the extra Fourier-space truncation associated with the fully-reduced model is included. It is fortuitous that in this idealized case the extra truncation actually inhibits an erroneous breakdown of the Rossby wave.

3.2 Localized initial conditions

The treatment of stable, localized structures has also been examined. Fig. 6 shows (upper left) an initial distribution of positive vorticity which as for the Rossby-Haurwitz wave has a maximum amplitude of Ω. The spatial variation of the vorticity is determined by a spectral fit to a field which is uniform outside the domain

$$\lambda_0 - \frac{\lambda_d}{2} < \lambda < \lambda_0 + \frac{\lambda_d}{2} \quad , \quad \theta_0 - \frac{\theta_d}{2} < \theta < \theta_0 + \frac{\theta_d}{2} \quad ,$$

and which varies within it as

$$\cos^2\left(\frac{\pi(\lambda - \lambda_0)}{\lambda_d}\right) \cos^2\left(\frac{\pi(\theta - \theta_0)}{\theta_d}\right)$$

We choose $\lambda_d = \theta_d = 22.5°$, $\lambda_0 = 90°$ and $\theta_0 = 60°$.

The integrations show that there is some initial dispersion of this vorticity field, but the prime feature is the setting up of a stable, circular vortex which slowly drifts northward and westward. Results at day 10 are shown in Fig. 6 from T106 runs with horizontal diffusion, for the Eulerian version using the full grid, the fully reduced grid and the fully reduced model, and for the semi-

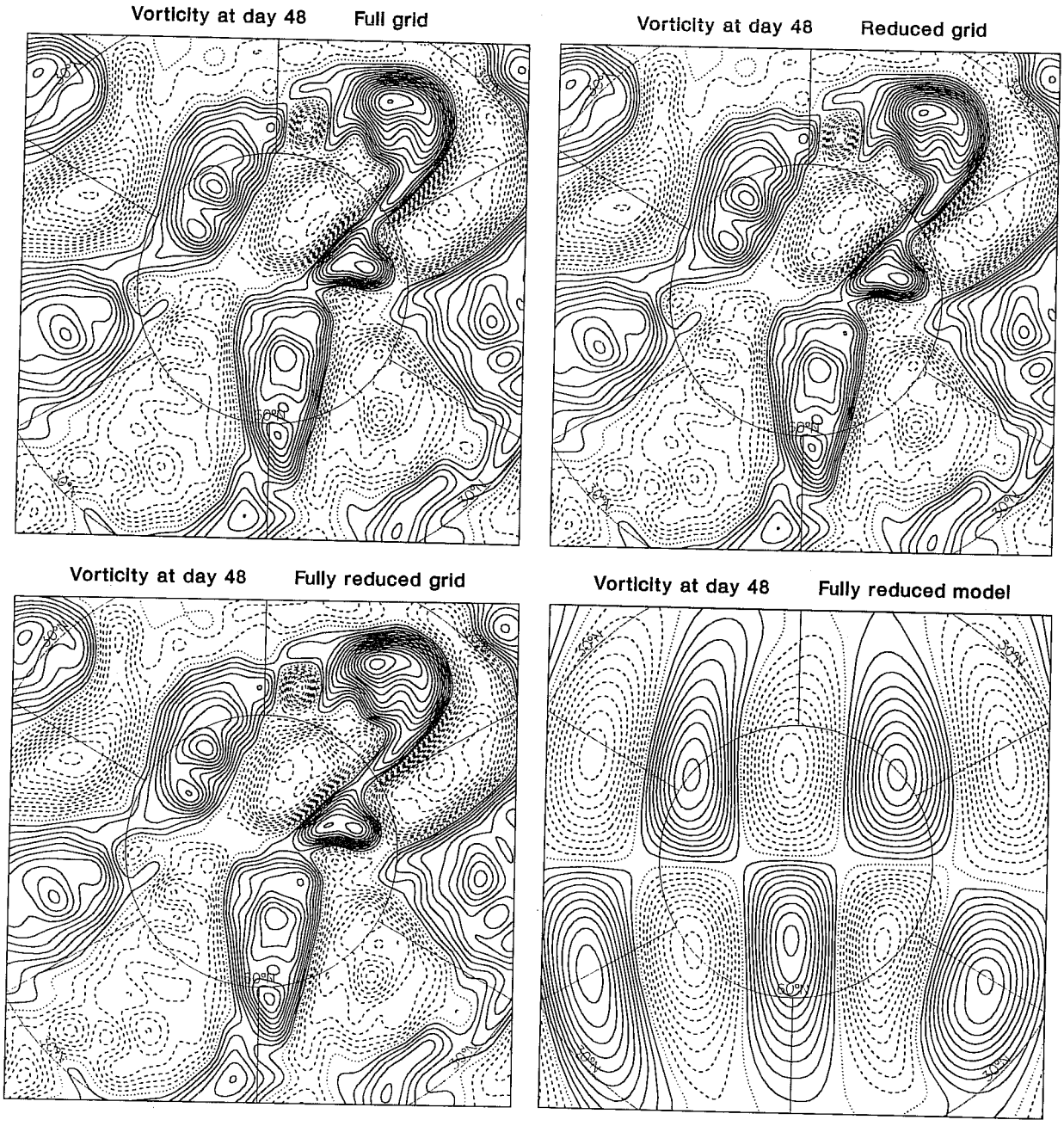

Fig. 5 The relative vorticity at day 48 produced using the full grid, the reduced grid, the fully reduced grid, and the fully reduced model, all at T42 resolution.

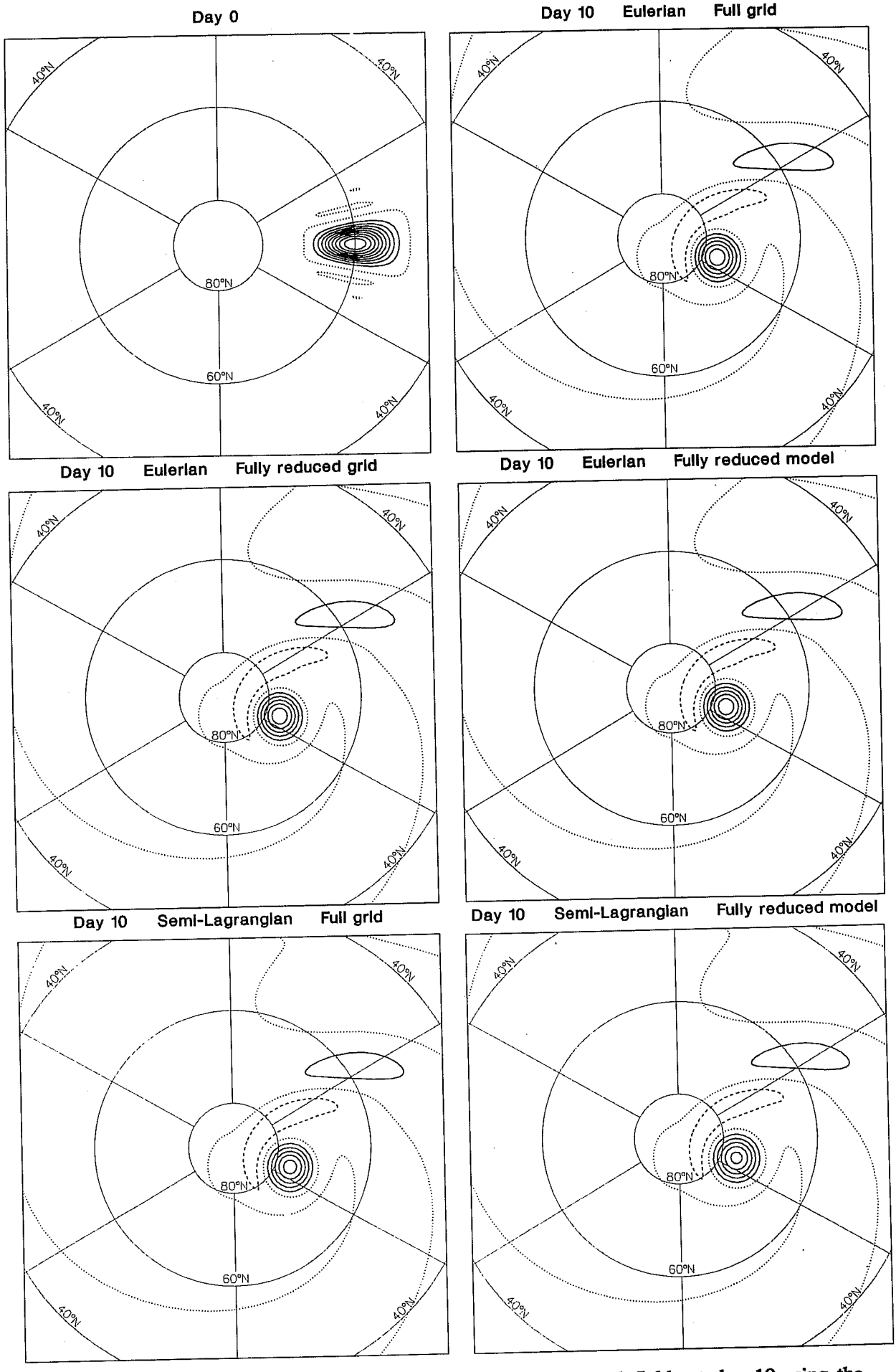

Fig. 6 An initial isolated distribution of relative vorticity, and fields at day 10 using the full grid, the fully reduced grid and the fully reduced model for Eulerian integrations, and the full grid and fully reduced model for semi-Lagrangian integrations. The resolution is T106.

Lagrangian version using the full grid and the fully reduced model. The Eulerian results are virtually indistinguishable, as is also the case when comparison is made with the corresponding integration using the reduced grid (not shown). The semi-Lagrangian forecasts are also highly similar, both to each other and to the Eulerian forecasts, although a very close inspection of the maps reveals a fractional loss of amplitude for the semi-Lagrangian version in the full grid case, and a very slight further loss for the fully reduced semi-Lagrangian model, due presumably to an increase in the damping associated with the interpolation of the vorticity field to the departure point in the case of the reduced grid. Given the 10-day range of the integration it is unlikely that such small differences are of any particular significance for the use of reduced grids (or semi-Lagrangian schemes) in numerical weather prediction.

3.3 Strong advection over the pole

The final case presented for the barotropic vorticity equation was devised to provide a test of the strong advection of a perturbation over the pole. Attention was particularly devoted to the semi-Lagrangian version of the model in this case. This was because of a suggestion by Williamson and Rasch (1989) that convergence of grid-points along latitude lines as the pole is approached may facilitate an accurate interpolation of vector wind components in the calculation of trajectories for the semi-Lagrangian advection.

The initial state comprises a large-scale flow and an isolated perturbation. The large-scale flow is specified by the vorticity distribution

$$\frac{2}{a} u_{max} (1 - 3\sin^2\theta')$$

where

$$\sin\theta' = \frac{1}{\sqrt{2}} (\cos\theta\cos\lambda + \sin\theta)$$

and a is the radius of the earth. This corresponds to a (0,2) spherical harmonic in a coordinate system in which the polar axis is inclined at 45° to the axis of rotation. The wave rotates westward without change in amplitude or shape with a frequency $\Omega/3$, and thus has a period very close to 3 days. The velocity maximum is u_{max}, which is here set to be 100 ms^{-1}, and this velocity occurs at the pole θ=90°.

The perturbation is of the form used in the preceding example but its initial location is given by λ_0=-120° and θ_0=50°, which positions it relative to the large-scale flow so as to ensure

advection over the pole θ=90°. Its initial maximum vorticity is 2Ω, and in the subsequent integration a maximum local velocity of 132ms^{-1} occurs. This stresses the stability of the Eulerian version of the model, and the timestep had to be reduced to 7.5 minutes for a stable T106 integration. The semi-Lagrangian integrations were carried out using the same one-hour timestep as used for the earlier examples.

Results after 18 and 36 hours of integration are shown in Fig. 7. The westward rotation of the large-scale pattern through approximately 90° in 18 hours can be clearly seen. The perturbation moves in a highly curved path, and after 18 hours has just crossed the pole. After 36 hours it is close to its starting latitude, and about 70° to the east of its starting longitude.

The plots in Fig. 7 are for the full-grid Eulerian and semi-Lagrangian calculations, and for the semi-Lagrangian calculations using the fully reduced model. All three integrations are very similar. A somewhat smaller amplitude to the perturbation in the semi-Lagrangian cases is the only obvious difference on these plots, although difference maps reveal also a slight phase difference between the Eulerian and semi-Lagrangian results. The semi-Lagrangian versions using the full grid and fully reduced model give remarkably similar results. It is necessary to examine such minute detail as the position of the dots in the negative contour east of the perturbation maximum to convince oneself that the two integrations really are different.

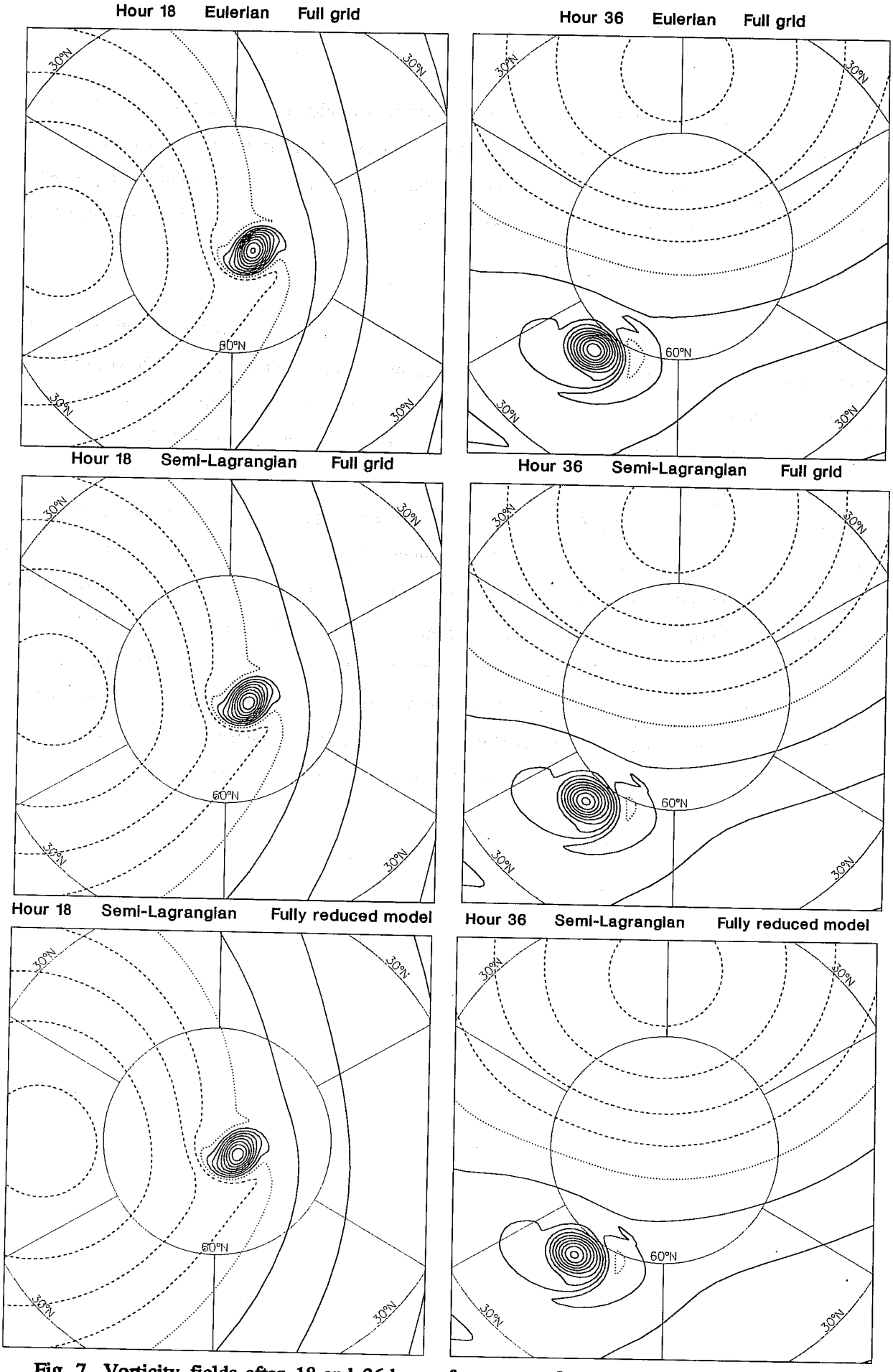

Fig. 7 Vorticity fields after 18 and 36 hours for a case of strong advection over the pole. Results are shown for an Eulerian full-grid integration and for semi-Lagrangian integrations using the full grid and fully reduced model. The contour interval in this case is $0.2\,\Omega$.

4. TEN-DAY FORECASTS

4.1 The reduced grid

A 10-day T106 forecast experiment using the reduced grid was carried out to provide a first indication of the viability of using a reduced number of longitude points in a complete medium-range prediction model. The use of the reduced grid was simulated by modifying the full operational ECMWF model so as to:

(i) use only zonal wavenumbers up to (NLN-1)/2 in the input to the inverse FFT at latitudes north of 60°N and south of 60°S, where NLN is the number of longitude points in the reduced grid at the latitude circle for which the transform is being performed;

(ii) use only the computed grid-point values from the longitude points that comprise the reduced grid as input to the direct FFT.

This enabled the meteorological impact (but not the impact on computational efficiency) of using the reduced grid to be assessed, although it should be noted that this first full test was not fully ideal in that the grid-point surface fields such as the land-sea mask and the orographic variances used in the parametrization of gravity-wave drag and calculation of the model's "envelope" orography were taken as their spot values from the full Gaussian grid, rather than being recomputed as values appropriate for the larger grid-boxes of the reduced grid.

4.2 The fully reduced grid

The model and its initial conditions were adapted to the fully reduced grid in such a way as to reproduce the full meteorological impact of the use of this grid, but not the full gain in computational efficiency. Thus vectorization of the code continued to be over the longitude points for individual model latitudes, giving short vectors in high latitudes. The record lengths used in the transfer of model data to and from secondary storage were kept the same for each latitude, so there was no saving either in I/O cost or in the secondary memory requirement of the model. Grid-point fields were interpolated to the full grid to enable use of standard archiving software, so a potential saving in the storage required for output fields was also not realized.

A further limitation to the gain in efficiency was the fact that in the standard model the full radiation calculation is performed only at every fourth point on each line of latitude, with FFTs used to provide fields at intermediate points. For the fully reduced grid, the full calculation was done at

(i) at a number of points per latitude which never exceeded the corresponding number used for the full grid (NLON/4: 80 for T106 resolution);

(ii) all points per row if their number was less than NLON/4;

(iii) every second, third or fourth point otherwise, as appropriate for the number of points in question.

This choice implies a further constraint on the number of points that can be used with the fully reduced grid, but the effect is a minor one. Table 1 shows where the number of points had to be changed for T106 resolution. For this resolution, the full radiation calculation was carried out at 17.1% fewer points for the fully reduced grid than for the full grid. A net saving of 19-20% in computational time was found when the fully reduced grid was used, with a further 2-3% coming from use of the fully reduced model.

The model land-sea distribution, orography, orographic variances and surface roughness lengths were recomputed for the fully reduced grid using the same 10′ resolution basic data as used in the corresponding computation for the operational full-grid model. Climatologies of deep-soil temperature and moisture used by the model were also recomputed. Other initial surface fields and boundary fields were constructed by linear interpolation from the full grid. Spherical-harmonic representations of the initial analysed upper-air fields (produced using the full-grid model in data assimilation) were used to evaluate fields on the fully reduced grid, and these fields were then interpolated vertically to account for the change in orography.

4.3 Results

Despite the less than ideal experimental set-up for the reduced grid, the impact of using it was extremely small. Anomaly correlations of 500hPa height are shown in Fig. 8 for the extratropical northern and southern hemispheres. The full-grid forecast which serves as the control for this experiment is the operational forecast of 15 July 1989. The scores presented in Fig. 8 and other objective verifications show that the two model versions are of highly comparable accuracy, and it is difficult to assign any significance to the small differences that can be seen.

Forecasts from 15 July 1989 have also been carried out using the fully reduced grid and the fully reduced model. Maps of the 500 hPa height over the European and Atlantic sectors of the high-latitude northern hemisphere are shown in Fig. 9 for the four 7-day forecasts for 22 July 1989, and for the analysis for this date. The forecasts are evidently all very similar, with especially close agreement between the full and reduced grids. Comparison with the analysis shows a

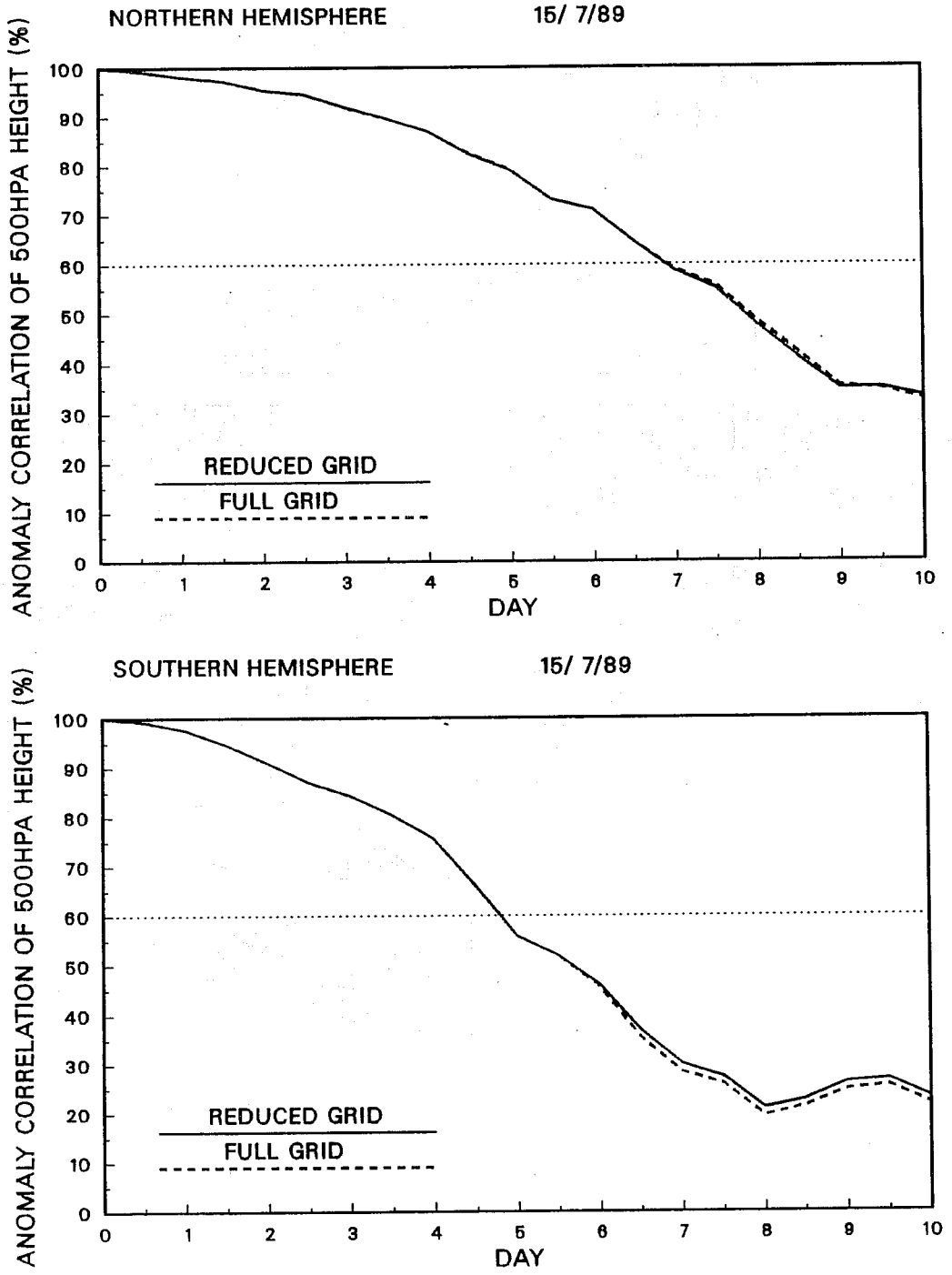

Fig. 8 Anomaly correlations of 500hPa height computed over the extratropical northern and southern hemispheres and for T106 forecasts from 12UTC 15 July 1989, using the reduced grid (solid lines) and the full grid (dashed lines).

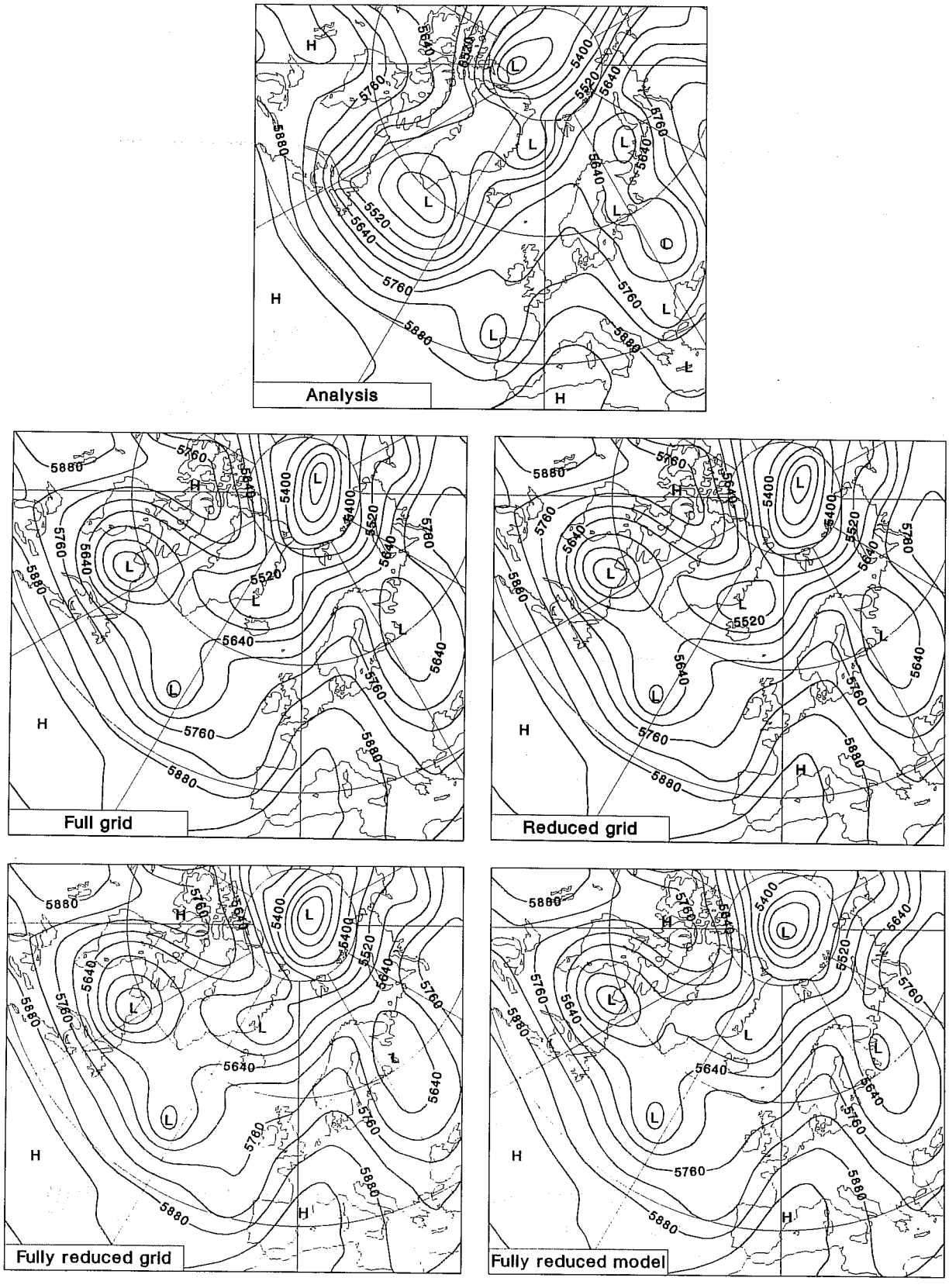

Fig. 9 The 500hPa height analysis (contour interval 60m) for 12UTC 22 July 1989 over the European and Atlantic sectors of the high-latitude northern hemisphere, and four day-7 forecasts verifying at this time.

broadly correct large-scale pattern in each case, and such differences as there are from forecast to forecast appear to be insignificant compared with the short-wave differences between any of the forecasts and the verifying analysis.

Corresponding maps for the Antarctic region are shown in Fig. 10. The objective verification shown in Fig. 8 indicates a significantly less accurate forecast in the southern than in the northern hemisphere at the 7-day range, and in Fig. 10 a major error is seen in the spurious cut-off low located east of the Antarctic Peninsula in each of the forecasts. The forecasts are generally very similar to each other, but the erroneous cut-offs produced using the fully reduced grid and model differ noticeably from those produced using the full and reduced grids.

The differences in the treatment of the erroneous cut-off are found to grow in place as the forecast range increases, and the differences occur principally between the pairs of forecasts that use different orographies, and different orographic variances in the parametrization of gravity-wave drag. This suggests that the differences may be due to the change in calculation of fixed model fields rather than any direct effect of using the coarser grid in the forecast. Indeed, the change in orography due to use of the fully reduced grid, shown in Fig. 11, is largest over the Antarctic Peninsula, where the difference just exceeds 300m. The largest difference in the northern hemisphere is about 235m, and occurs over the southern tip of Greenland. It can also be seen in Fig. 11 that the orography for the fully reduced grid is predominantly higher than that for the full grid. This is a consequence of the use of envelope orographies which are computed using grid-square means and sub-gridscale variances calculated for the apprpriate computational grid using the 10′ resolution input data. The convergence of the grid-length near the poles for the full grid implies a lower variance for this grid than for the fully reduced grid. The Antarctic Peninsula and southern Andes were the regions of the southern hemisphere that were the most sensitive to a change from mean to envelope orography in experiments at resolutions above T21 reported by Jarraud et al. (1988).

Forecasts with the fully reduced grid have also been carried out for three other cases, with initial dates 15 October and 15 December 1989, and 15 February 1990, and comparison has been made with standard full-grid forecasts from these dates. Anomaly correlations of 500hPa height averaged over the four available cases are shown in Fig. 12 for the extratropical northern and southern hemispheres. The two sets of forecasts are basically very similar with a slight advantage to the fully reduced grid for the northern hemisphere, and differences which vary with the forecast range for the (less accurate) southern hemispheric forecasts. This picture is found

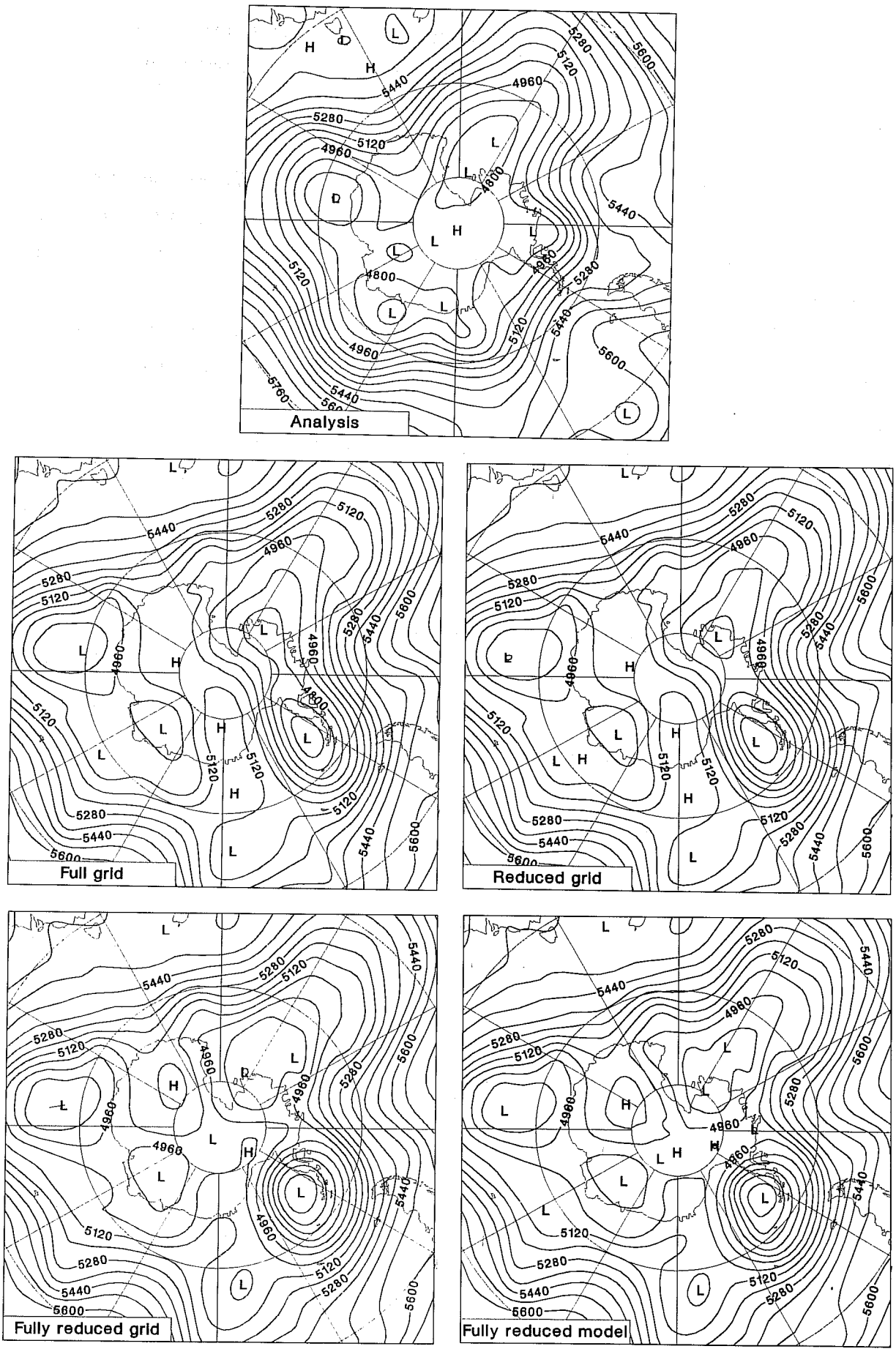

Fig.10 The 500hPa height analysis (contour interval 60m) for 12UTC 22 July 1989 over the Antarctic region, and four day-7 forecasts verifying at this time.

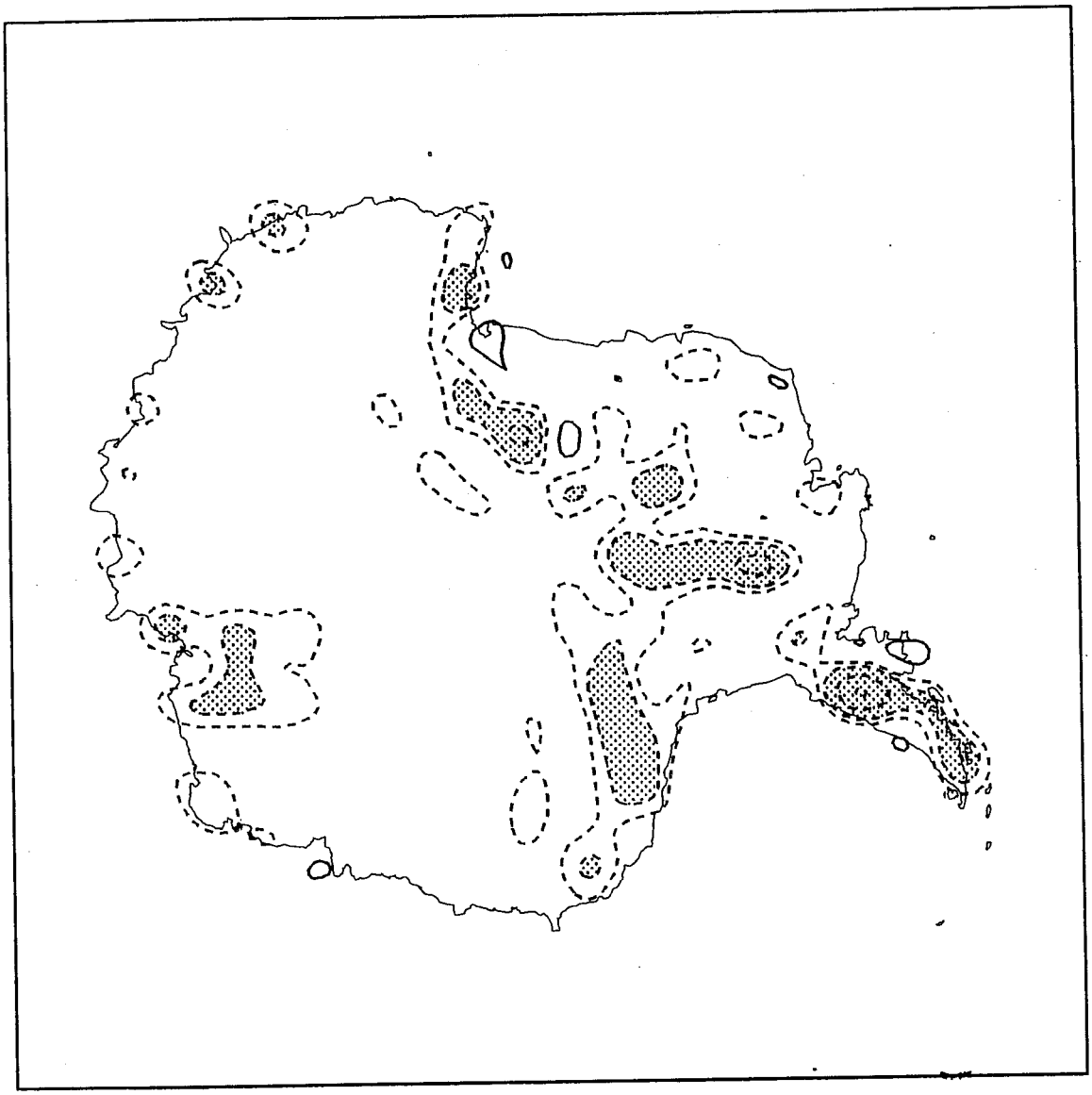

Fig.11 The difference in Antarctic orography between that computed for the full grid and that for the fully reduced grid. Contours are drawn at 50, 100, 200 and 300m, with regions where differences exceed 100m shaded. Dashed contours denote where the orography of the fully reduced grid is higher than that of the full grid.

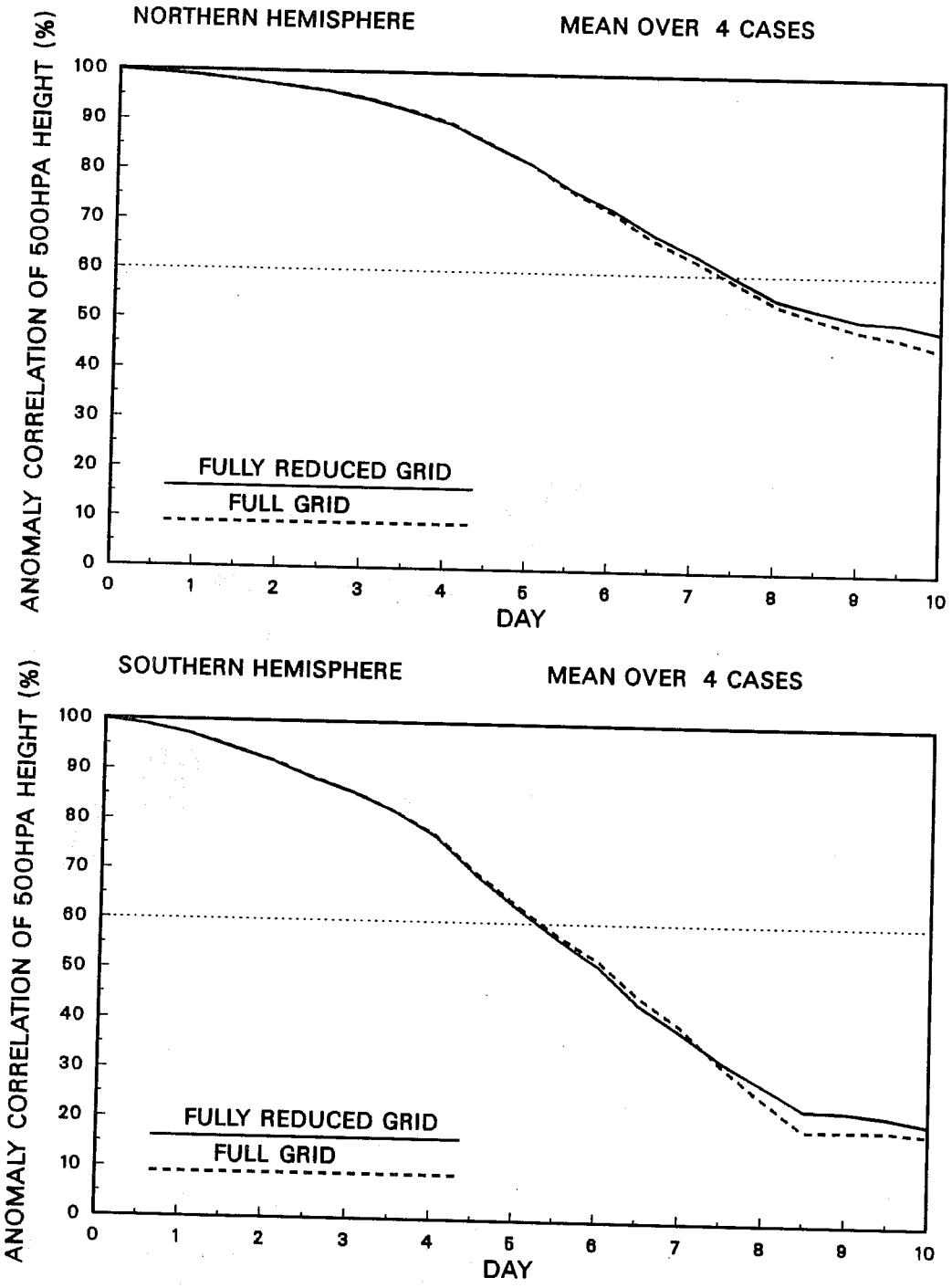

Fig.12 Anomaly correlations of 500hPa height computed over the extratropical northern and southern hemispheres and averaged over four T106 forecasts, for the fully reduced grid (solid lines) and the full grid (dashed lines).

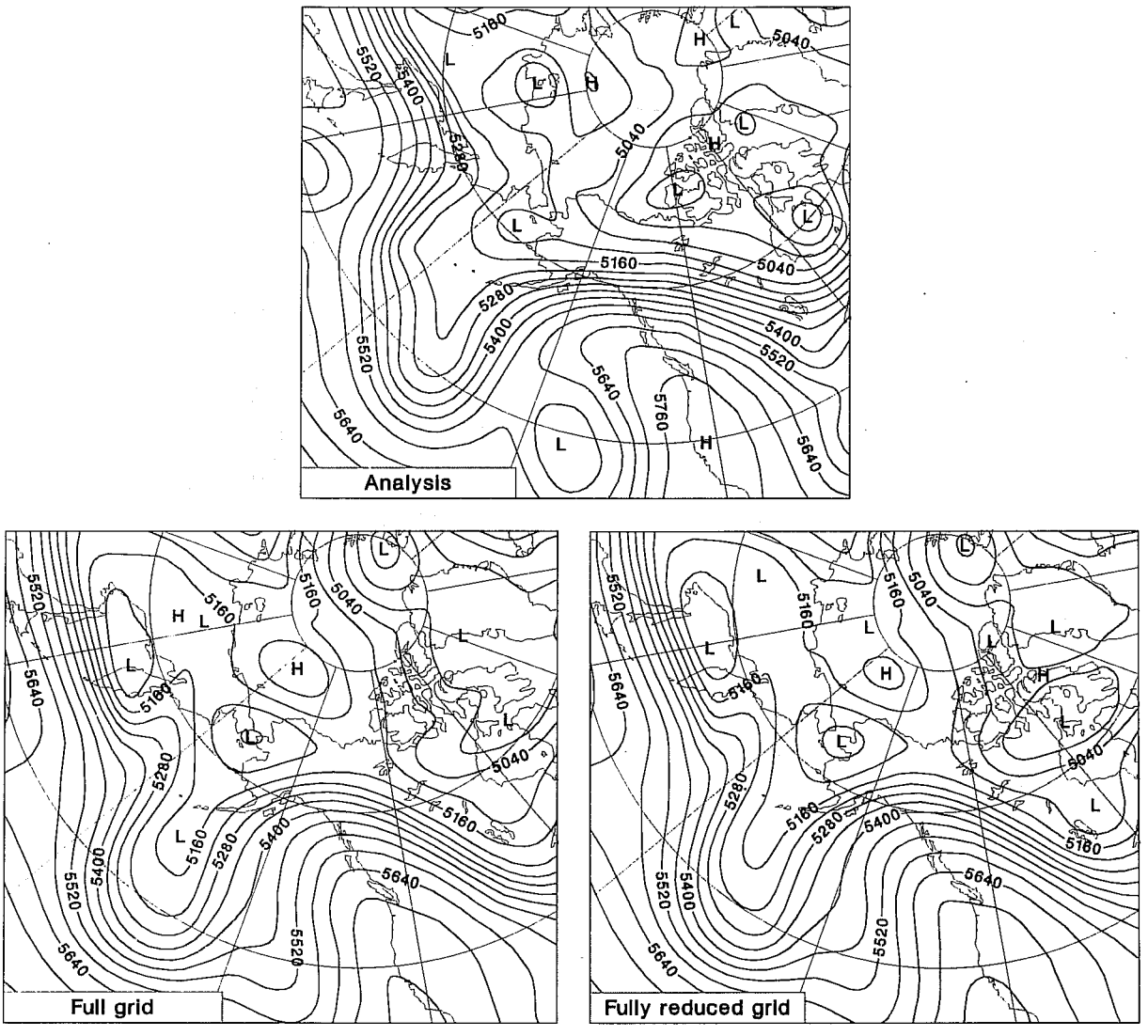

Fig.13 The 500hPa height analysis (contour interval 60m) for 12UTC 22 February 1990 over the Pacific sector of the high-latitude northern hemisphere, and day-7 forecasts for this time using the full and fully reduced grids.

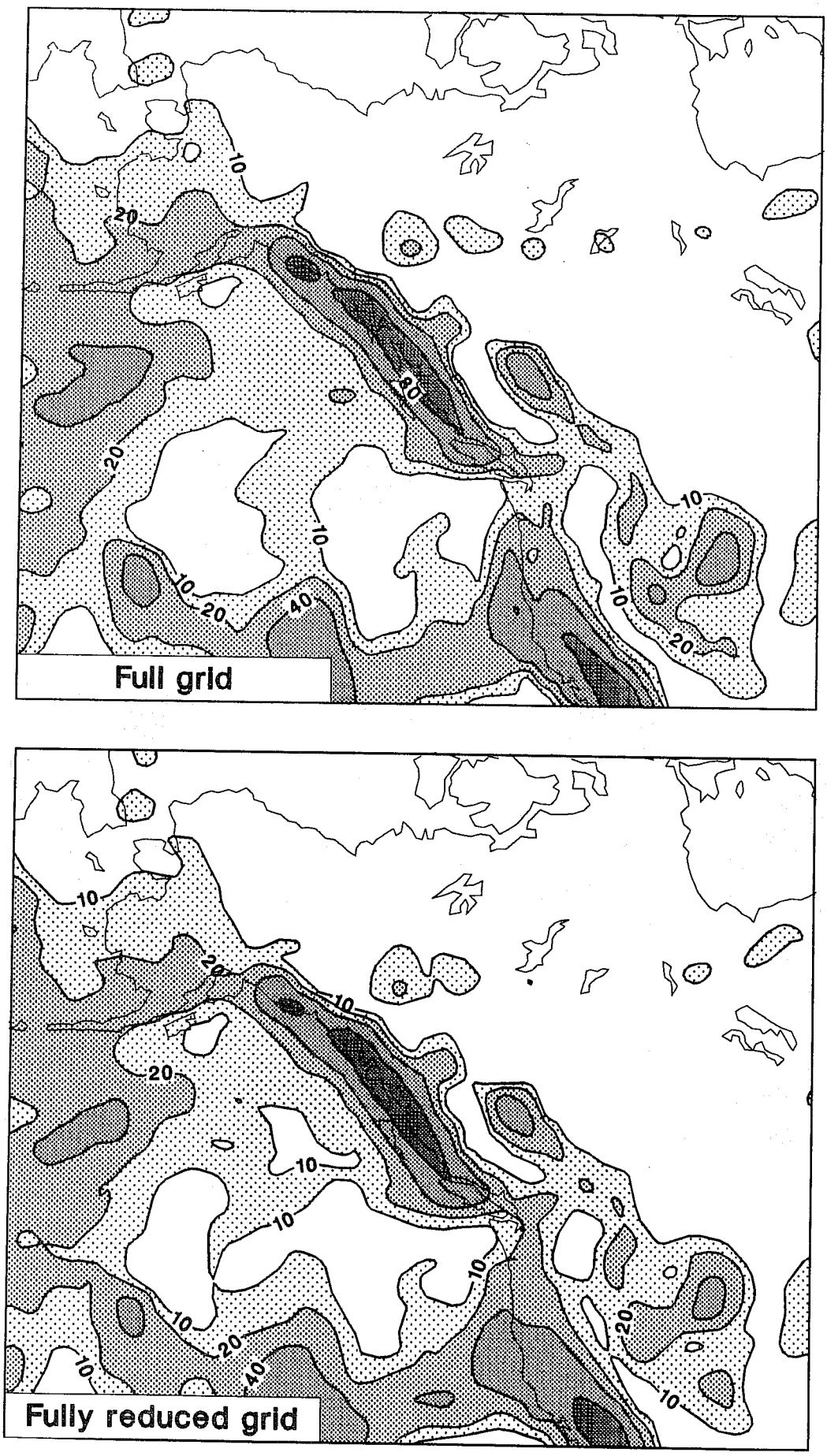

Fig. 14 Precipitation accumulated over the first 7 days of forecasts using the full and fully reduced grids. The initial time and date was 12 UTC 15 February 1990, and results are shown over northwestern North America and the surrounding ocean. Contour intervals are 10, 20, 40 and 80mm.

for other verification scores, fields and levels for the extratropics; scores for the tropics are, not surprisingly, highly similar. The number of cases studied is not sufficient to determine whether such differences are representative, or merely a product of limited sampling. There is, however, certainly no evidence of any general lowering of forecast accuracy due to use of the fully reduced grid, and the use of grid-squares of fairly uniform size for the calculation of variances may have given a slight overall advantage to the forecasts using the fully reduced grid.

Day-7 forecasts of 500hPa height for the high-latitude Pacific sector of the northern hemisphere are shown in Fig. 13 for the February case. This was again one of good large-scale forecast accuracy for this hemisphere, and the results from the full grid and the fully reduced grid can be seen to be very similar. Such similarity occurs also for fields other than the 500hPa height. A concluding example is shown in Fig. 14, which presents the 7-day accumulated precipitation over northwestern North America and the neighbouring ocean, also for the February case. Data for the fully-reduced grid was interpolated linearly to the full grid prior to plotting, which tends to reduce maxima slightly. Despite this, there is again a high degree of similarity between the two forecasts, and this extends to a number of quite small-scale features.

5. DISCUSSION

The results presented in this paper indicate that there are indeed savings to be made by running spectral models with less than the full Gaussian grid, with no significant loss of accuracy. This has been shown for both idealized integrations and medium-range weather forecasts at T106 resolution. We have found a saving in excess of 20% in the computational cost of the current T106 ECMWF forecast model, without making any particular effort to optimize the code. The saving for any particular model will depend on the proportion of the model calculation that is carried out in grid-point space. We expect a larger saving to be achieved in a semi-Lagrangian version of the ECMWF model which is currently under development, since in this version there is an increase in the amount of grid-point calculation per timestep, and a reduction in the number of Legendre transforms (Temperton, 1990).

In addition to the forecast experiments presented in preceding sections, a 90-day T42 simulation has also been carried out using the fully reduced model. Differences from a full-grid integration were larger over the initial 10-day range than found in the T106 experiments, though still small compared with the errors of either forecast. Mean maps for longer time ranges show some differences, but these are not unduly large. In particular, 90-day mean extratropical 500hPa heights from the two simulations show essentially the same patterns of difference from the corresponding mean of analysed heights. Such differences as do occur may be due to orographic differences or simulated natural variability, rather than directly due to the difference in grid. Further experimentation is needed to establish the suitability of reduced grids for climate studies, but our initial results are promising.

The fact that sensitivity to the change in grid is larger at T42 than at T106 resolution, and the figures quoted in Section 2 with regard to the comparison of orographies, lead us to expect that differences between forecasts using the full and fully reduced grids will be even smaller at the higher horizontal resolutions that will shortly be introduced operationally at a number of forecasting centres. It has been shown that sub-gridscale orographic variances can be significantly larger at high latitudes when calculated using the fully reduced rather than the full grid, and if these are used to define an envelope orography, then this orography is higher than the corresponding orography computed using the standard grid. Use of such an enhanced orography may be detrimental at lower resolutions, since Jarraud et al. (1988) found a worsening of T42 and T63 summer forecasts over the northern hemisphere due to use of envelope orography at high latitudes.

The reductions in grid considered here are different from (and complementary to) that considered by Côté and Staniforth (1988), who showed for a two-time-level semi-Lagrangian model that a general reduction in resolution of the Gaussian grid could be employed without loss of stability or accuracy in T126 integrations of the shallow water equations. The extent to which such an overall reduction in resolution may be used in a multi-level model with realistic orography requires investigation, since in this case the non-advective terms are more highly non-linear, particularly the pressure-gradient term which largely balances the geopotential gradient over steeply sloping ground in terrain-following coordinates. Of particular interest would be a study of the combination of the fully reduced grid considered here and an overall reduction in grid-resolution of the type (if not the extent) discussed by Côté and Staniforth.

Acknowledgements

We are particularly grateful to H.Ritchie for making available to us the code of his semi-Lagrangian spectral shallow-water model, and for advice on its use in this study. We thank also D.Williamson for comments on this work, and R. Mureau for suggested improvements to the text.

References

Asselin, R., 1972: Frequency filter for time integrations. Mon. Wea. Rev., 100, 487-490.

Côté, J. and A. Staniforth, 1988: A two-time-level semi-Lagrangian semi-implicit scheme for spectral models. Mon. Wea. Rev.,116, 2003-2012.

Eliasen, E., B. Machenhauer and E. Rasmussen, 1970: On a numerical method for integration of the hydrodynamical equations with a spectral representation of the horizontal fields. Inst. of Theor. Met., Univ. of Copenhagen, Report No. 2.

Hoskins, B.J., 1973: Stability of the Rossby-Haurwitz wave. Quart. J. Roy. Met. Soc., 99, 723-745.

Jarraud, M., A.J. Simmons and M. Kanamitsu, 1988: Sensitivity of medium range weather forecasts to the use of an envelope orography. Quart. J. Roy. Met. Soc., 114, 989-1025.

Kurihara, Y., 1965: Numerical integration of the primitive equations on a spherical grid. Mon. Wea. Rev., 93, 399-415.

Machenhauer, B., 1979: The spectral method. GARP Publication Series No. 17, Vol 2, 121-275.

Orszag, S.A., 1970: Transform method for calculation of vector coupled sums: application to the spectral form of the vorticity equation. J. Atmos. Sci., 27, 890-895.

Ritchie, H., 1988: Application of the semi-Lagrangian method to a spectral model of the shallow water equations. Mon. Wea. Rev., 116, 1587-1598.

Simmons, A.J., and M. Jarraud, 1984: The design and performance of the new ECMWF operational model. Proceedings of 1983 ECMWF Seminar on Numerical Methods for Weather Prediction, Vol. 2, 113-164.

Simmons, A.J., D.M. Burridge, M. Jarraud, C. Girard and W. Wergen, 1989: The ECMWF medium-range prediction models. Development of the numerical formulations and the impact of increased resolution. Meteor. Atmos. Phys., 40, 28-60.

Temperton, C., 1990: A note on scalar and vector transform methods for global spectral models. Submitted to Mon. Wea. Rev..

Williamson, D.L., and P.J. Rasch, 1989: Two-dimensional semi-Lagrangian transport with shape-preserving interpolation. Mon. Wea. Rev., 117, 102-129.